



<http://www.diva-portal.org>

Postprint

This is the accepted version of a paper published in *The Journal of Physical Chemistry C*. This paper has been peer-reviewed but does not include the final publisher proof-corrections or journal pagination.

Citation for the original published paper (version of record):

Pazoki, M., Taghavinia, N., Hagfeldt, A., Boschloo, G. (2014)
Mesoporous TiO₂ Microbead Electrodes for Cobalt-Mediator-Based Dye-Sensitized Solar Cells.
The Journal of Physical Chemistry C, 118(30): 16472-16478
<http://dx.doi.org/10.1021/jp4113574>

Access to the published version may require subscription.

N.B. When citing this work, cite the original published paper.

Permanent link to this version:

<http://urn.kb.se/resolve?urn=urn:nbn:se:uu:diva-231290>

Mesoporous TiO₂ Microbead Electrodes for Cobalt-mediator based Dye-Sensitized Solar Cells

Meysam Pazoki^{†‡}, Nima Taghavinia[†], Anders Hagfeldt[‡] and Gerrit Boschloo^{‡*}

[†]Department of Physics, Sharif University of Technology, Box 11155-9161, Tehran, Iran

[‡] Department of Chemistry - Ångström Laboratory, Uppsala University, Box 523, SE 75120 Uppsala, Sweden

ABSTRACT

Light scattering, porosity, surface area and morphology of TiO₂ working electrode can affect the power conversion efficiency of dye sensitized solar cells dramatically. Here, mesoporous TiO₂ microbeads were tested as working electrode in dye-sensitized solar cells based on cobalt tris-bipyridine electrolyte. Power conversion efficiencies (PCE) up to 6.4% were obtained with D35 dye adsorbed onto the light-scattering microbeads. Electron transport, studied using small light perturbation methods, was found to be significantly faster in the microbead films than in standard mesoporous TiO₂ films. This was attributed to the favorable assembly of nanocrystals in the microbeads, which can increase the electron diffusion coefficient in the conduction band. Electron lifetimes were similar in both types of film. While solar cell performance of microbead

films was comparable to that of standard mesoporous films in acetonitrile-based electrolytes, a significant improvement was found when the more viscous 3-methoxypropionitrile was used as solvent for electrolyte.

KEYWORDS: Tris(2,2'-bipyridine)cobalt(II), TiO₂ Microbeads, Dye-sensitization

INTRODUCTION

Dye-sensitized solar cells (DSCs) have attracted much attention in recent years because of their potential for low-cost production, flexibility in design and colors and their good performance, especially under low-light conditions.^{1,2} In the DSC, dye molecules are adsorbed in a monolayer on the high internal surface area of a mesoporous titanium dioxide film, which is deposited on a conducting substrate. A liquid electrolyte containing a redox couple fills the pores of the electrode and has as function to reduce the dye after photoinduced electron injection into TiO₂, as well as to conduct positive charge to the counter electrode.

Until recently, iodide / triiodide was the only redox mediator in DSC that gave good solar cell results, but recently several promising alternatives have been developed, namely cobalt complexes,³⁻⁹ copper complexes, ferrocene,¹⁰ disulfide/thiolate systems,¹¹ nickel bis(dicarbollide),¹² as well as solid-state alternatives with the molecular hole conductor spiroOMeTAD.^{13,14} Most promising are perhaps the cobalt complexes. Recently, a record efficiency for DSC of 12.4% was obtained using a cobalt mediator by Grätzel and co-workers.⁷ Cobalt mediators absorb less light than triiodide and their redox potential can be tuned by using different ligands and by chemical

modification of these ligands.³⁻⁹ Mass transport of cobalt mediators can be a problem in the DSC due to their relatively large size and their limited solubility compared to iodide/triiodide redox couple.^{5,156}

The morphology of the TiO₂ film can affect mass transport of the redox mediators in the DSC. Specifically, N.-G. Park and co-workers demonstrated that the porosity and the pore size of mesoporous TiO₂ films strongly affected the mass transport of cobalt tris bipyridyl in the pores of the working electrode, resulting in significant changes in the DSC performance.¹⁶

In this paper, we report on the application of titanium dioxide mesoporous microbeads in dye-sensitized solar cells with cobalt electrolytes. TiO₂ microbead electrodes have great potential for DSC, yielding efficiencies of more than 10% in iodide/triiodide electrolyte.¹⁷⁻²⁰ The good performance is attributed to a large internal surface area of the microbeads and good light-scattering properties. Koo et al. prepared hollow TiO₂ microspheres with diameters of 1 to 3 micrometer with a wall thickness of 250 nm.¹⁷ Caruso and co-workers prepared monodisperse microbeads with tunable pore size by controlled hydrolysis of a titanium precursor in the presence of hexadecylamine.^{18,19} Resulting microbeads were about 830 nm in size, with a pore diameter in the range of 14 to 23 nm. Kim et al. prepared mesoporous 250 nm-sized TiO₂ beads using controlled hydrolysis without the use of surfactants.²⁰ They reported that the bead structure was not always maintained in the resulting sintered films. Pan et al. synthesized mesoporous microbeads with different pore sizes of 6.5, 8.2 and 11.0 nm and studied the effect of pore size for the DSCs with iodide/ triiodide based electrolyte.²¹ Miao et al. used microbeads as scattering layer in iodide-electrolyte based DSCs and obtained 7.94 % efficiency.²² There are some reports on the fast charge transport inside the microbead electrodes,^{19,22} which can be beneficial for the

solar cell performance. The combination of TiO₂ nanoparticles with good electron transporting materials such as TiO₂ nanobelts or pillars can improve the electron transport in a film, but this goes at the expense of surface area of the film.^{23,24} In the mesoporous microbeads faster transport is accompanied with a high surface area and good light reflecting properties.

Here we have applied for the first time mesoporous TiO₂ microbead electrodes in cobalt electrolyte based DSCs and studied the light harvesting, redox diffusion and electron transport in the fabricated DSCs. The mesoporous microbead structure, with a controlled mesopore size inside the bead and much larger pores in between the beads, appears to be an ideal structure for DSC with cobalt-based electrolytes, as the diffusion of the redox mediator is expected to be improved in this porous electrode.

EXPERIMENTAL SECTION

Synthesis of microbeads: TiO₂ mesoporous microbeads were synthesized by a combination of sol-gel and solvothermal methods as developed by Chen et al.¹⁸ Briefly, hexadecylamine (1.37 g) that acts as structure directing agent was dissolved in ethanol (200 mL), and 0.8 mL of a 0.1 M aqueous KCl solution was added, controlling the ionic strength in the solution. Titanium(IV)isopropoxide (Aldrich97%, 4.4 mL) was added under vigorous stirring at room temperature, and the solution was left standing for 18h. Finally, the solution was centrifuged and dried at room temperature. Solvothermal treatment: the TiO₂ beads were dispersed in a mixture of 20 mL ethanol and 10 mL deionized (DI) water and adding of 1 mL ammonia solution (Merck,25% in water). The solution was transferred into a teflon-lined pressure vessel and kept for 17 hours at 167 °C in a furnace. Finally, the suspension was centrifuged and the microbeads

were dried in air at room temperature. A screen-printable paste was prepared by mixing 1 gram of TiO₂ microbead powder with 3.2 gram of 10% wt solution of ethylcellulose in terpineol and 0.2 mL acetic acid in 11mL ethanol. The solution was stirred by magnetic stirrer at room temperature until solvent evaporated and a viscous paste was obtained.

Solar cell fabrication: Fluorine doped tin oxide coated glass (FTO, TEC 15 from Pilkington) was cleaned by ultrasonication in, respectively, detergent, DI water, 0.1 M HCl in ethanol, acetone and ethanol, for 30 minutes each, with DI water rinsing between each step. Substrates were immersed in an aqueous solution of 40mM TiCl₄ for 1 hour at 70°C, rinsed with DI water and ethanol and dried in a nitrogen gas flow. Deposition of TiO₂ microbead paste and standard mesoporous TiO₂ paste (Dyesol 18NR-T) on the FTO was done by screen printing using a mesh size of 180 micron and 5 mm times 5 mm squares. Then the TiO₂ films was kept 5 minutes in ethanol atmosphere and dried at 125°C between each print. The electrodes were sintered in air using a furnace (10 minutes at 180°C, 10 minutes at 320°C, 10 minutes at 390°C and 30 minutes at 490°C; ramp time between each step was 30 min). For the second TiCl₄ treatment the films were immersed in a 20 mM TiCl₄ aqueous solution for 30 minutes at 70°C and sintered at 490°C for 20 minutes. After cooling to 80°C, working electrodes were immersed and kept overnight in a 0.2 mM ethanolic solution of D35dye(((E)-3-(5-(4-(bis(20,40-dibutoxybiphenyl-4-yl)amino)phenyl)thiophen-2-yl)-2-cyanoacrylic acid). After dye adsorption, electrodes were briefly rinsed using ethanol and dried in vacuum. Counter electrodes were fabricated as follows: Hole drilled FTO cleaned as mentioned before, sintered at 400°C for 15 minutes, covered by a droplet of 5 mM ethanolic solution of H₂PtCl₆ and heated again in 400°C for 15 minutes. The working and counter electrodes were sealed using a thermoplastic frame (Surlyn, 40 μm thickness). The electrolyte was introduced through the hole of counter electrode by vacuum

backfilling, and the hole was sealed using thermoplastic and a glass slide. The electrolyte used in this work consists of 0.22 M $\text{Co}(\text{bpy})_3(\text{PF}_6)_2$, 0.05 M $\text{Co}(\text{bpy})_3(\text{PF}_6)_3$, 0.1M LiClO_4 and 0.2M tert-butylpyridine in acetonitrile (ACN) or 3-methoxypropionitrile (MPN).

Characterization of TiO_2 material: Surface morphology and crystalline phase was studied using scanning electron microscopy (Hitachi model S-4160) and X-ray diffraction (Siemens model D5000). Thickness of the films was measured using a profilometer (Dektak 3). Optical transmission and reflection spectra of TiO_2 films were obtained using a UV-vis-NIR spectrophotometer with integrating sphere (Cary5000).

Characterization of DSCs: The current-voltage characteristics of the DSCs were recorded by Keithley 2400 source/meter under AM 1.5 conditions from solar Newport simulator model 91160 calibrated with a silicon diode. A black square mask with 36 mm^2 area was used for current - voltage measurements. For measurements in different light intensities, neutral density filters (Thorlab) were used. The Incident Photon to Current Efficiency (IPCE) of the cells was recorded using a xenon light source (Spectral Products ASBXE - 175), a monochromator (Spectral Products CM110), and a Keithley 2700 multimeter. Electron lifetime and transport time were recorded by recording the transient of voltage and current of the cell in the response of small amplitude square wave perturbations at working conditions in different light intensities. The light was generated by a white LED and current and voltages were recorded using a digital acquisition board. The amount of extracted charge at open circuit and short circuit conditions were measured by biasing the LED light, keeping the cell in the desired working condition for 10 seconds and finally turning the light off and integrating the current versus time for 15 seconds. Short circuit Fermi level was measured by method introduced elsewhere.¹² Dye was desorbed

from films using 0.1M tetrabutylammonium hydroxide in methanol and the UV-vis absorption of the solution was measured (Ocean Optics HR 2000) to determine the dye load.

RESULTS AND DISCUSSION

Figure 1 shows SEM micrographs of the synthesized TiO₂ microbeads. Initially, smooth spheres are grown by the sol-gel method (Figure 1a), which after the solvothermal treatment transform into microbeads: mesoporous spheres consisting of nanoparticles (Figure 1b,c). During the sol-gel synthesis, hydrolysis of titanium isopropoxide results in Ti(OCH(CH₃)₂)_{4-x}(OH)_x species and their oligomers, which can make hydrogen-bonds interactions with amino groups of the HDA and form small inorganic-organic composites that self-organize into rod-like micelles and finally into microporous beads.²⁵ Initially formed amorphous particles crystallize to the anatase nanocrystals with very high surface area after solvothermal treatment in 167°C.²⁵

The diameter of the initially formed spheres was about 900 nm, which reduced to 800 nm after solvothermal treatment. Figure 1c shows a high resolution image of the surface of a microbead, revealing ~20 nm sized features, demonstrating the nanocrystalline nature of the microbeads. X-ray diffraction of the microbeads confirms formation of a nanocrystalline TiO₂anatase phase (see Figure S.2 of supporting information). Using the Debye-Scherrer formula a crystallite size of 12 nm was calculated from the broadening of the (101) peak. A cross-section of a sintered microbead film (a single printed layer) is shown in Figure 1d. The microbead structure is fully maintained throughout the film. However, when using slightly different preparation conditions, partial collapse of the microbead structure could occur. Figure S3(in supporting information) shows an example where the microbead structure collapsed in part of the film adjacent to the

substrate. For the remainder of this paper, only results from films where the microbead structure was maintained will be discussed.

Microbead films have a bright white opaque appearance. The size of the microbeads (800 nm) is such that they will scatter visible light strongly.²⁶ The optical properties of microbead films with a thickness of 10 micrometer were measured in a spectrometer equipped with an integrating sphere, see Figure 2. The total (diffuse plus specular) reflectance is about 50-60 % in the wavelength range of 400 to 800 nm. Upon immersion in a dye bath (D35), the films become strongly colored, clearly indicating that the microbeads are mesoporous. The reflectance drops strongly in the range where the dye absorbs light to about 5 %. This signifies that the reflectance is not so strong that light absorption by the dye is prevented, but instead light-scattering takes place in the whole volume of the 10 μm film, allowing for good light absorption by the dye. The total transmittance is close to zero up to 550 nm.

The dye loading of microbead films was studied using dye adsorption - desorption experiments with the organic dye D35, see Figure 3. As expected, there is a linear relation between the amount of dye adsorbed and the film thickness. The slope was determined to be $1.0 \times 10^{-8} \text{ mol cm}^{-2} \mu\text{m}^{-1}$. For comparison, the dyeload of a conventional transparent mesoporous TiO_2 film (Dyesol 18NR-T, 5.8 μm thickness) was also determined and was found to be $9.7 \times 10^{-8} \text{ mol cm}^{-2}$, which is about 70% higher than that of a microbead film with the same thickness. The N_2 -BET area and porosity of the Dyesol 18NR-T film was determined to be $61.8 \text{ m}^2\text{g}^{-1}$ and 64%, respectively. It can thus be calculated that a D35 molecule occupies an area of 0.85 nm^2 on the TiO_2 surface, which suggests a close packing of the molecule. The roughness factor (real surface

area/projected area) of the mesoporous film is calculated to be $85\mu\text{m}^{-1}$, while that of the microbead film is $60\mu\text{m}^{-1}$. The lower dye load and roughness factor of the microbead films can be ascribed to the higher porosity of the microbead film, due to the large voids present in between the beads.

Dye-sensitized solar cells were prepared using TiO_2 microbead electrodes, D35 sensitizer and a cobalt tris-bipyridine based redox electrolyte in acetonitrile. Results of the current-voltage characterization under AM1.5G solar irradiation (100 mW cm^{-2}) are summarized in Table 1 and Figure 4a. The optimum microbead film thickness is about $12\mu\text{m}$, where both the efficiency (η) and short-circuit current density (J_{SC}) show a maximum. The open-circuit potential (V_{OC}) shows a gradual decrease with film thickness d . Comparison with a standard mesoporous TiO_2 electrode reveals that J_{SC} and solar cell efficiency is higher for the $5.8\mu\text{m}$ 18NR-T film compared to a microbead film of similar thickness. However, comparing with a microbead film of $7.8\mu\text{m}$ that has approximately the same dye load (and TiO_2 content), a similar photocurrent density and solar cell efficiency is found. The V_{OC} is higher for the microbead films.

Incident photon-to-photocurrent efficiency (IPCE) spectra of the cells are shown in Figure 4b. The IPCE increases in the absorption maximum up to a film thickness of $12\mu\text{m}$. Further increase of d resulted in a slight improvement of the IPCE in the red part of the spectrum (see Figure S1 in supporting information for normalized IPCE spectra). Integration of the IPCE spectra multiplied by the spectral AM1.5G solar photon flux in the range 350 nm to 800 nm yielded theoretical J_{SC} values that were in good accordance with the experimental values, except for 3L, where the calculated value (11.3 mA cm^{-2}) was 20% higher than the experimental value. This can

be attributed to electron losses at higher light intensities due to limitations in the mass transport in the electrolyte, as will be discussed later.

Electron transport and recombination in the solar cells was investigated using small modulation square wave perturbation techniques. In Figure 5 the electron lifetime and transport time of the solar cells are shown. Similar lifetimes were found for standard mesoporous (5.8 μm) and microbead (7.8 μm) films, which is not surprising considering that they have similar surface area (with calculated roughness factors of 490 and 470, respectively) and give similar photocurrent densities. The electron transport time measured under short-circuit conditions was, however, significantly faster for the microbead films than for standard mesoporous electrodes, see Figure 5b. We attribute the faster transport in microbead film to more favorable connections between the nanocrystals in the mesoporous structure of the microbeads that are formed during hydrothermal treatment, resulting in a higher effective diffusion coefficient for electrons.

The relation between charge and open-circuit potential was investigated using a charge extraction method. In Figure 6a the $Q_{\text{OC}} - V_{\text{OC}}$ relation for microbead films with two thicknesses is compared to that of a mesoporous TiO_2 electrode. As expected, the extracted charge scales with film thickness for the two microbead films. The charge of the standard mesoporous film (5.8 μm) was slightly higher than that of a microbead film with similar TiO_2 content ($d = 7.8 \mu\text{m}$). The charge varies exponentially with open circuit voltage, which is consistent with the multiple trapping model for charge transport in dye-sensitized solar cells, where an exponential distribution of trap states below the conduction band edge is assumed. For a trap distribution $g(V) = g_0 \exp(V/m)$, the density of trap states n_t is given by:

$$n_t = mg_0 \left[\exp\left(\frac{V}{m}\right) - 1 \right] \text{ (Eq. 1),}$$

where g_0 is the trap density at $V=0$ V and m the slope of the exponential trap distribution. The slope differs significantly between standard mesoporous electrodes ($m= 0.10$ eV) and microbead electrodes ($m= 0.12$ eV). Furthermore, g_0 is larger for the microbeads.

Figure 6b shows the short-circuit charge Q_{SC} and the internal potential V_{SC} in microbead and standard mesoporous films as function of short circuit current density. The trends are quite similar. The internal potential, corresponding to the average quasi-Fermi level in the porous TiO_2 film under short circuit conditions, is about -0.65 V versus the redox potential of the electrolyte or -0.13 V vs NHE. Comparison with the lifetime data in Fig. 5a demonstrates that the electron lifetime under short circuit conditions is very high, more than 1 s, so that electron losses to the electrolyte can be neglected under these conditions. The Q_{SC} and V_{SC} are slightly less for the 7.8 μm microbead solar cell compared to the 5.8 μm 18NR-T film, so that the density of conduction band electrons is expected to be slightly less for the microbead solar cell. Nevertheless, it was found that electron transport was faster for this solar cell. Following the multiple trapping model, which assumes only transport of conduction band electrons, this implies that the diffusion coefficient for electrons in the conduction band of TiO_2 in microbead films is significantly higher than in standard mesoporous TiO_2 films. As both type of film have the same crystalline phase (TiO_2 anatase), this suggests that the effect of grain boundaries is included in the electron diffusion coefficient in the conduction band. The determined values are much lower than that in an anatase single crystal.

Mass transport in the electrolyte of microbead solar cells is expected to be better than in solar cells with standard mesoporous TiO₂ film, due to the presence of large pores in between the microbeads. In low-viscous acetonitrile-based electrolytes, however, no significant effects due to improved mass transport were. To further investigate the effect of mass transport, a series of solar cells was prepared using a cobalt-complex based electrolyte with the more viscous solvent 3-methoxypropionitrile. The solar cell performance of these devices was good at low light intensities with efficiencies of about 5-6% at 1/10th of a sun for standard mesoporous films and up to 7% for microbead films, decreasing to 2.5 - 4% for standard mesoporous films and about 4.5 % for mesoporous films(see Figure S5 in supporting information). The linearity of short circuit current versus light intensity is much better for DSCs based on microbead films than those based on standard mesoporous films, see Figure 7. The photocurrent reaches a limiting value of about 12 mAcm⁻² in the microbead DSCs in MPN (data not shown), while a value of about 8 mAcm⁻² is found for the standard mesoporous films. This strongly indicates that insufficient diffusion of Co(III) species in the pores of the standard mesoporous film is a major limitation for the photocurrent. The diffusion coefficient of Co(bpy)₃³⁺ in the mesoporous structure was found to be much smaller than that in bulk electrolyte.¹⁵ The significantly improved mass transport of Co(bpy)₃³⁺ in microbead-based DSC with MPN based electrolyte, can be explained by the large pores between the beads.

Preliminary results on use of microbead films as scattering films on top of transparent mesoporous films appear very promising (see Table S1 and Figure S6). Also mixing of microbeads with standard mesoporous TiO₂ paste has yielded promising results, where the scattering microbeads improve the devices performance.

In conclusion, TiO₂ microbead electrodes were successfully applied in dye-sensitized solar cells with cobalt-based electrolyte. Mass transport in the pores of the microbead film was improved significantly, because of the large pores in between the single microbead particles. Furthermore, the diffusion coefficient of conduction band electrons appears to be higher in the microbead films

ASSOCIATED CONTENT

Supporting Information. Normalized IPCE spectra of the cells; XRD pattern of microbead electrode; Microbeads as light scattering layer in DSC. This material is available free of charge via the Internet at <http://pubs.acs.org>.

AUTHOR INFORMATION

Corresponding Author

* Email: gerrit.boschloo@kemi.uu.se

ACKNOWLEDGMENTS

We thank the Swedish Energy Agency, the Swedish Research Council, the STandUP for Energy program, the Iran ministry of science and technology and the European Community's Seventh Framework Programme (FP7/2007-2013 under grant agreement n° 246124 of the SANS project) for financial support. We thank Leif Häggman for SEM measurements and Majid Safdari for BET measurements.

Table 1. Solar cell characteristics of dye-sensitized solar cells with TiO₂ microbead photoanodes and cobalt-based electrolyte.^{a,b}

Device ^c	Film thickness (μm)	V _{oc} (V)	J _{sc} (mAcm ⁻²)	FF (%)	η(%)
1L_diluted	4.5	0.93	6.9	61	3.9
1L	7.8	0.90	9.2	65	5.4
2L	11.9	0.88	10.8	67	6.4
3L	17	0.87	9.6	67	5.6
18NR-T	5.8	0.88	9.4	60	5.0

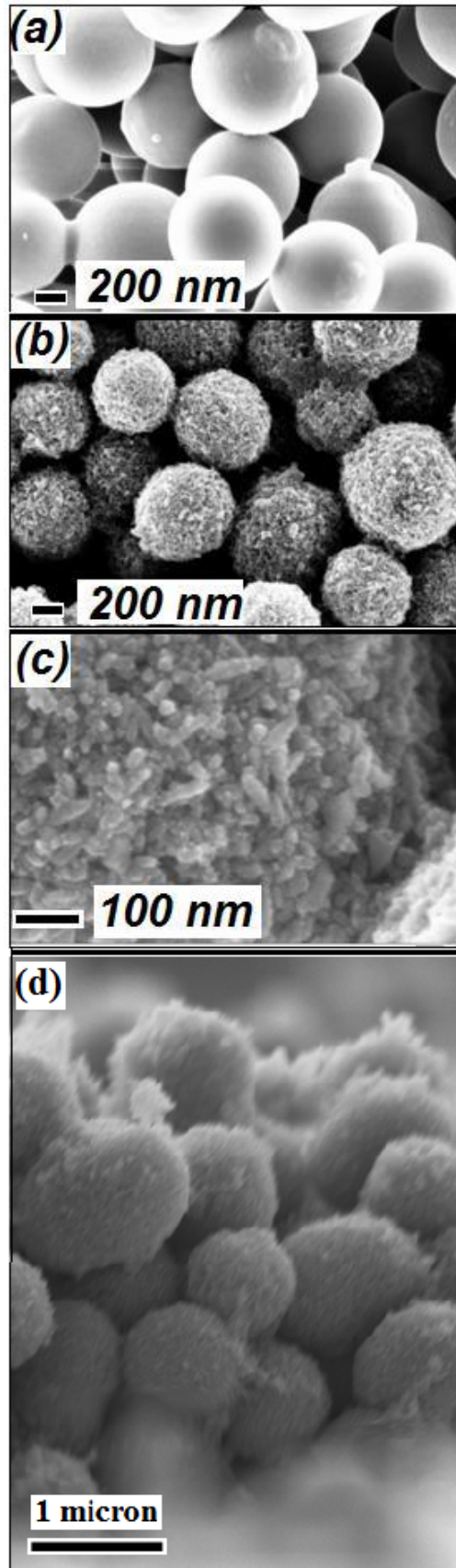
a) Irradiance 100 mW cm⁻² AM1.5G.

b) Electrolyte: 0.22 M Co(bpy)₃(PF₆)₂, 0.05 M Co(bpy)₃(PF₆)₃, 0.1M LiClO₄ and 0.2M tert-butylpyridine in acetonitrile.

c) 1L_diluted = device with microbead layer from one print with diluted paste; 1L = 1 layer microbead paste; 2L = 2 layers, etc. 18NR-T: device with standard mesoporous TiO₂.

Figures

Figure 1. Scanning electron microscope pictures of sol-gel synthesized amorphous TiO₂ spheres (a), crystalline microbeads obtained after solvothermal treatment (b), and a high resolution image of the microbead surface (c). Cross-section of a sintered microbead film (d).



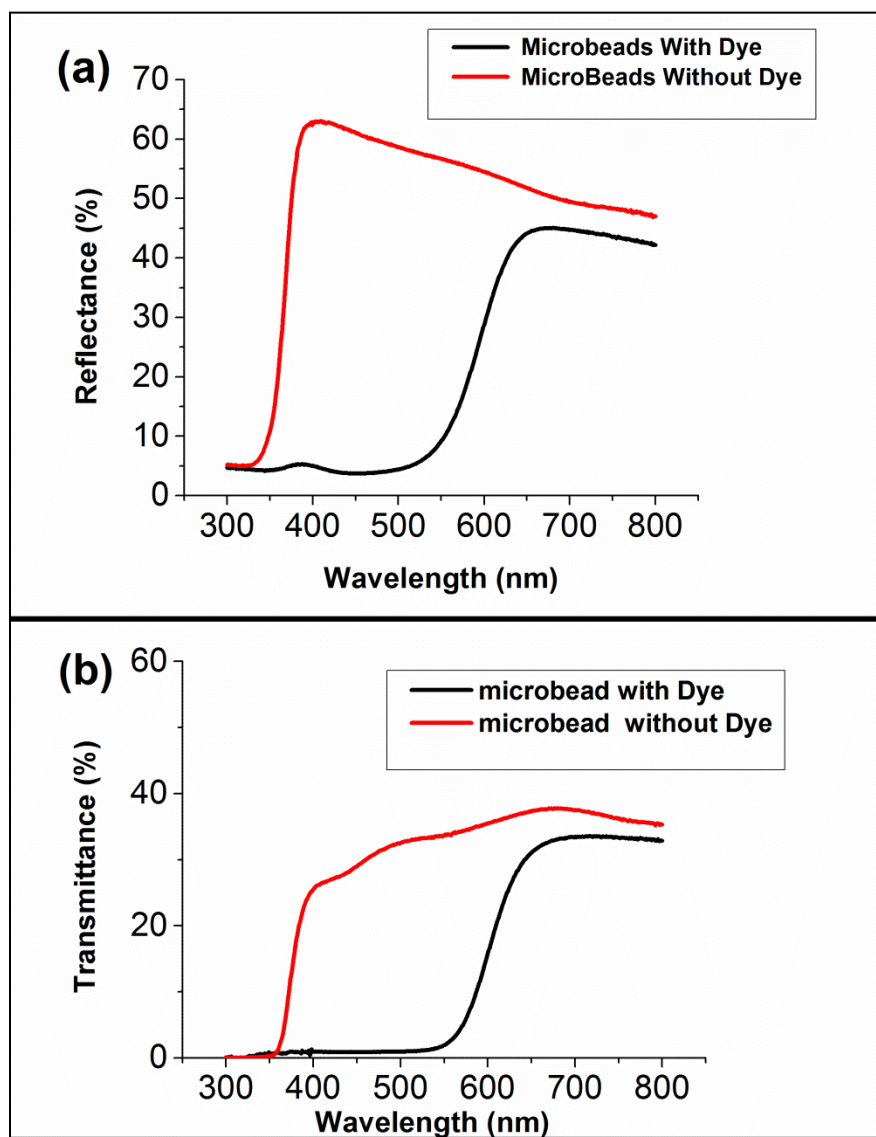


Figure 2.Total (a) reflectance and (b) transmittance of TiO₂ microbead films, with and without modification with adsorbed D35 dye molecules. The film thickness was 10 μm.

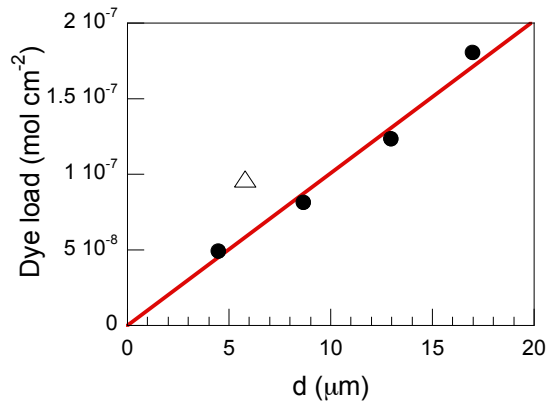


Figure 3.D35 dye load of TiO₂ microbead electrodes as function of film thickness. The slope of the linear regression fit is $1.0 \times 10^{-8} \text{ mol cm}^{-2} \mu\text{m}^{-1}$. The triangle represents the dye load of a standard mesoporous TiO₂ film (Dyesol 18NR -T).

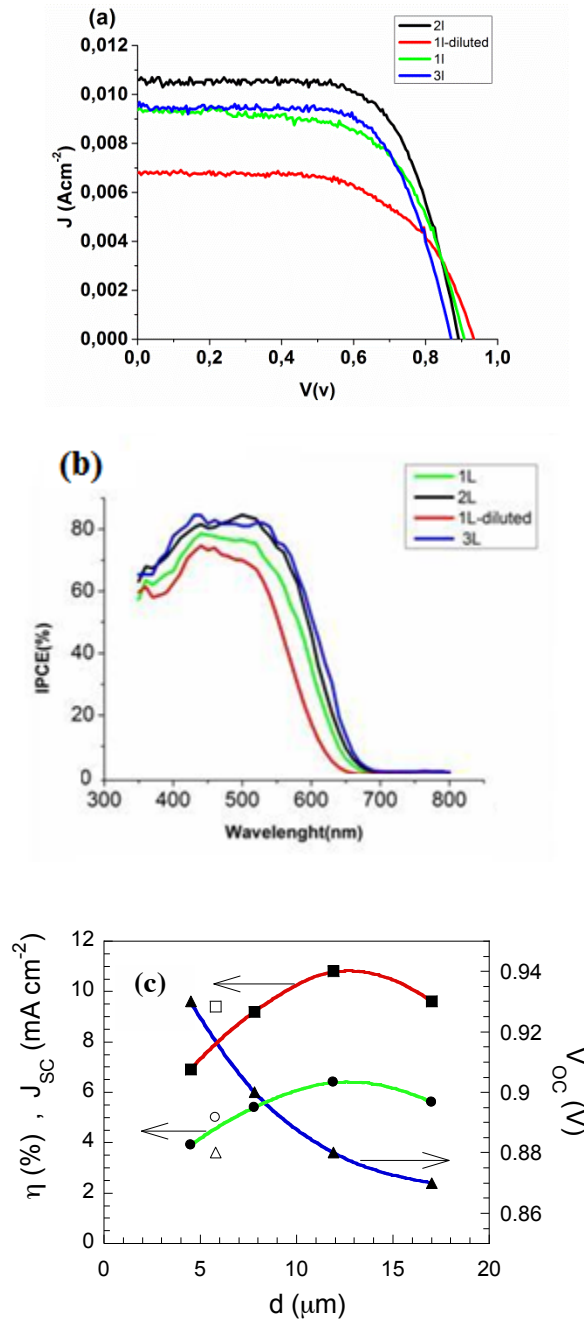


Figure 4. Solar cell characteristics of TiO₂ microbead-based dye-sensitized solar cells in cobalt-based electrolytes. (a) Current density – voltage curves under 1 sun illumination. (b) IPCE spectra. (c) Characteristic solar cell parameters as function of film thickness. J_{sc} (Squares),

efficiency (η , circles) and V_{OC} (triangles) are shown. Closed symbols represent microbead films, open symbols 18NR-T film.

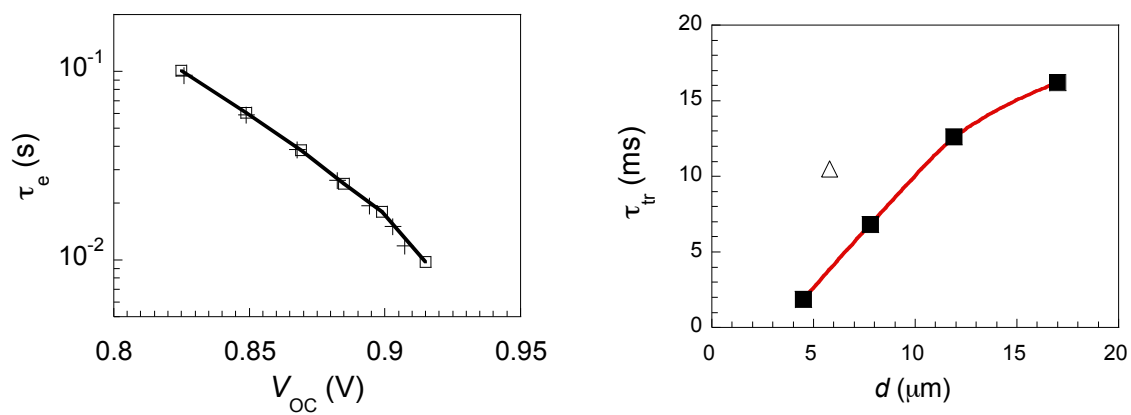


Figure 5. (a) Electron lifetime as function of open circuit potential. 18NR-T (crosses) and 1L (squares). (b) Electron transport time at $J_{SC} = 1 \text{ mA cm}^{-2}$ as a function of film thickness of microbead solar cells (filled symbols) and 18NR-T (triangle). The lines are guides to the eye.

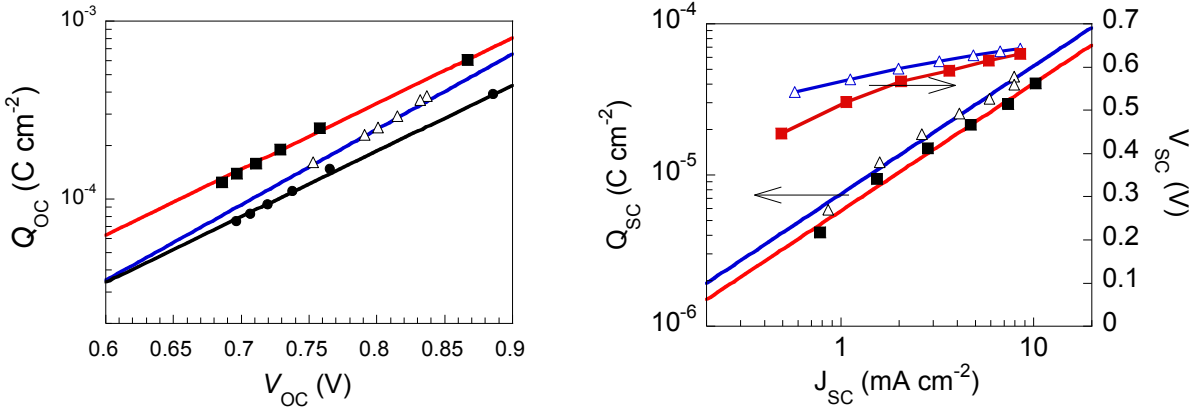


Figure 6. (a) Charge-potential relation in microbead cells (filled symbols) and standard mesoporous TiO_2 cells (open triangles). The drawn lines correspond to fits to Eq. 1. (b) Extracted charge under short circuit conditions and internal potential in the DSCs as function of J_{SC} .

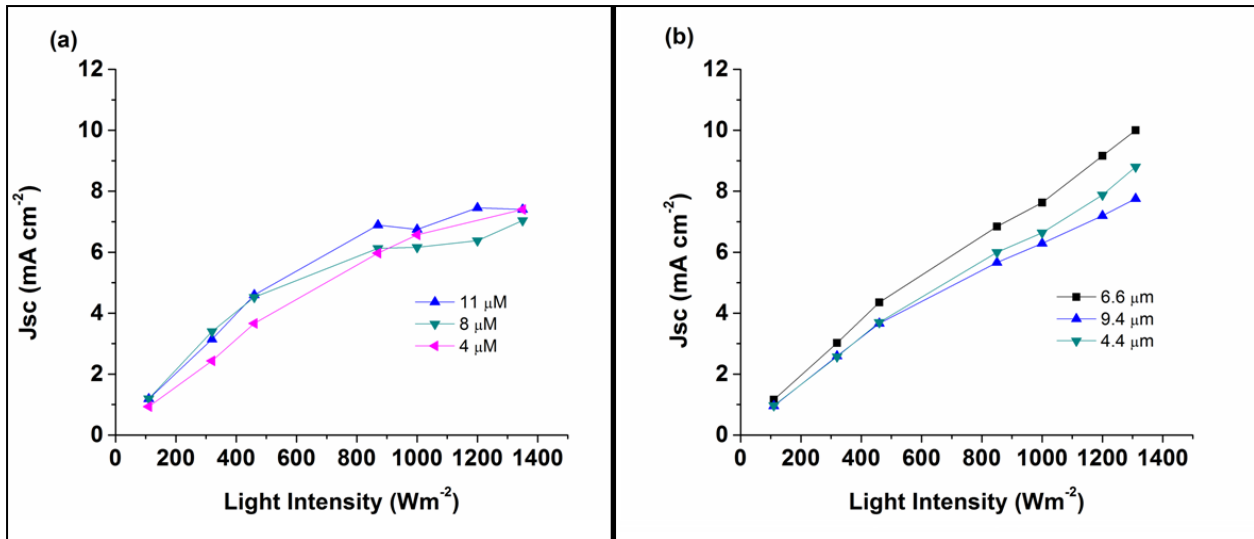


Figure 7. Short-circuit current density of (a) standard mesoporous TiO_2 films and (b) microbead films as function of light intensity for D35-sensitized solar cells with MPN-based cobalt bipyridine electrolyte.

REFERENCES

- (1) Hagfeldt, A.; Boschloo, G.; Sun, L.; Kloo, L.; Pettersson, H. Dye-Sensitized Solar Cells. *Chem. Rev.* **2010**, *110*, 6595.
- (2) O'Regan, B.; Grätzel, M. A low-cost, high-efficiency solar cell based on dye-sensitized colloidal TiO₂ films. *Nature* **1991**, *353*, 737-740.
- (3) Sapp, S. A.; Elliott, C. M.; Contado, C.; Caramori, S.; Bignozzi, C. A. Substituted Polypyridine Complexes of Cobalt(II/III) as Efficient Electron-Transfer Mediators in Dye-Sensitized Solar Cells. *J. Am. Chem. Soc.* **2002**, *124*, 11215-11222.
- (4) Nusbaumer, H.; Moser, J.-E.; Zakeeruddin, S. M.; Nazeeruddin, M. K.; Grätzel, M. Co^{II}(dbbip)₂²⁺ Complex Rivals Tri-iodide/Iodide Redox Mediator in Dye-Sensitized Photovoltaic Cells. *J. Phys. Chem. B* **2001**, *105*, 10461-10464.
- (5) Klahr, B. M.; Hamann, T. W. J. Performance Enhancement and Limitations of Cobalt Bipyridyl Redox Shuttles in Dye-Sensitized Solar Cells. *Phys. Chem. C* **2009**, *113*, 14040.
- (6) Feldt, S. M.; Gibson, E. A.; Gabrielsson, E.; Sun, L.; Boschloo, G.; Hagfeldt, A. Design of Organic dyes and Cobalt Polypyridine Redox Mediators for high-Efficiency Dye-Sensitized Solar Cells. *J. Am. Chem. Soc.* **2010**, *132*, 16714.
- (7) Yella, A.; Lee, H.-W.; Tsao, H. N.; Yi, C.; Chandiran, A. K.; Nazeeruddin, M. K.; Diao, E. W.-G.; Yeh, C.-Y.; Zakeeruddin, S. M.; Grätzel, M. Porphyrin-Sensitized Solar Cells with Cobalt(II/III) Redox Electrolyte Exceeds 12 percent Efficiency. *Science* **2011**, *334*, 629-634.
- (8) Feldt, S. M.; Wang, G.; Boschloo, G.; Hagfeldt, A. Effects of Driving Forces for Recombination and Regeneration on the Photovoltaic Performance of Dye-Sensitized Solar Cells using Cobalt Polypyridine Redox Couples. *J. Phys. Chem. C* **2011**, *115*, 21500-21507.
- (9) Yum, J.-H.; Baranoff, E.; Kessler, F.; Moehl, T.; Ahmad, S.; Bessho, T.; Marchioro, A.; Ghadiri, E.; Moser, J.-E.; Yi, C.; Nazeeruddin, M. K.; Grätzel, M. A cobalt complex redox shuttle for dye-sensitized solar cells with high open-circuit potentials. *Nat. Commun.* **2012**, *3*, 631.
- (10) Daeneke, T.; Kwon, T.-H.; Holmes, A. B.; Duffy, N. W.; Bach, U.; Spiccia, L. High-Efficiency dye-sensitized solar cells with ferrocene-based electrolytes. *Nat. Chem.* **2011**, *3*, 211.
- (11) Wang, M.; Chamberland, N.; Breau, L.; Moser, J.-E.; Humphry-Baker, R.; Marsan, B.; Zakeeruddin, S. M.; Grätzel, M. An Organic Redox Electrolyte to rival Triiodide/Iodide in Dye-Sensitized Solar Cells. *Nat. Chem.* **2010**, *2*, 385.
- (12) Li, T. C.; Spokoyny, A. M.; She, C.; Farha, O. K.; Mirkin, C. A.; Marks, T. J.; Hupp, J. T. Ni(III)/(IV) Bis(dicarbollide) as Fast, Noncorrosive Redox Shuttle for Dye-Sensitized Solar Cells. *J. Am. Chem. Soc.* **2010**, *132*, 4580.
- (13) Bach, U.; Lupo, D.; Comte, P.; Moser, J. E.; Weissortel, F.; Salbeck, J.; Spreitzer, H.; Grätzel, M. Solid-State Dye-Sensitized Mesoporous TiO₂ Solar Cells with High Photon-to-Electron Conversion Efficiencies. *Nature* **1998**, *395*, 583-585.
- (14) Burschka, J.; Dualeh, A.; Kessler, F.; Baranoff, E.; Cevey-Ha, N.-L.; Yi, C.; Nazeeruddin, M. K.; Grätzel, M. Tris(2-(1H-pyrazol-1-yl)pyridine) Cobalt(III) as p-Type Dopant for Organic Semiconductors and Its Application in Highly Efficient Solid-State Dye-Sensitized Solar Cells. *J. Am. Chem. Soc.* **2011**, *133*, 18042-18045.
- (15) Nelson, J. J.; Amick, T. J.; Elliott, C. M. Mass Transport of Polypyridyl Cobalt Complexes in Dye-Sensitized Solar Cells with Mesoporous TiO₂ Photoanodes. *J. Phys. Chem. C* **2008**, *112*, 18255.

- (16) Kim, H.-S.; Ko, S.-B.; Jang, I.-H.; Park, N.-G. Improvement of Mass Transport of the $[\text{Co}(\text{bpy})_3]^{II/III}$ Redox Couple by Controlling Nanostructure of TiO_2 Films in Dye-Sensitized Solar Cells. *Chem. Commun.* **2011**, 47, 12637.
- (17) Koo, H. J.; Kim, Y. J.; Lee, Y. H.; Lee, W. I.; Kim, K.; Park, N.-G. Nano-embossed Hollow Spherical TiO_2 as Bifunctional Material for High-Efficiency Dye-Sensitized Solar Cells. *Adv. Mater.* **2008**, 20, 195.
- (18) Chen, D.; Huang, F.; Cheng, Y.-B.; Caruso, R. A. Mesoporous Anatase TiO_2 Beads with High Surface Areas and Controllable Pore Sizes: A Superior Candidate for High-Performance Dye-Sensitized Solar Cells. *Adv. Mater.* **2009**, 21, 2206.
- (19) Sauvage, F.; Chen, D.; Comte, P.; Huang, F.; Heiniger, L.-P.; Cheng, Y.-B.; Caruso, R. A.; Grätzel, M. Dye-Sensitized Solar Cells Employing a Single Film of Mesoporous TiO_2 Beads Achieve Power Conversion Efficiencies. Over 10% *ACS Nano* **2010**, 4, 4420-4425.
- (20) Kim, Y. J.; Lee, M. H.; Kim, H. J.; Lim, G.; Choi, Y. S.; Park, N.-G.; Kim, K.; Lee, W. I. Formation of Highly Efficient Dye-Sensitized Solar Cells by Hierarchical Pore Generation with Nanoporous TiO_2 Spheres. *Adv. Mater.* **2009**, 21, 3668.
- (21) Pan, K. et al. Dye-Sensitized Solar Cells Based on Large-Pore Mesoporous TiO_2 with Controllable Pore Diameters. *Eur. J. Inorg. Chem.* **2011**, 30, 4730
- (22) Miao, X.; Pan, K.; Liao, Y.; Zhou, W.; Pan, Q.; Tian, G.; and Wang, G. Controlled Synthesis of Mesoporous Anatase TiO_2 Microspheres as a Scattering Layer to Enhance the Photoelectrical Conversion Efficiency. *J. Mater. Chem. A* **2013**, 1, 9853.
- (23) Pan, K.; Dong, Y.; Tian, C.; Zhou, W.; Tian, G.; Zhao, B.; and Fu, H. TiO_2 -B Nanobelt/Anatase TiO_2 Nanoparticle Heterophase Nanostructure fabricated by Layer-by-Layer Assembly for High-Efficiency Dye-Sensitized Solar Cells. *Electrochimica Acta* 2009, 54, 7350.
- (24) Zhaung, G. et al. Anatase TiO_2 Pillar-Nanoparticle Composite fabricated by Layer-by-Layer Assembly for High-Efficiency Dye-Sensitized Solar Cells. *Dalton Transactions* **2012**, 41, 12683.
- (25) Chen, D.; Cao, L.; Huang, F.; Imperia, P.; Cheng, Y.; and Caruso, R.A. Synthesis of Monodisperse Mesoporous Titania Beads with Controllable Diameter, High Surface Areas, and Variable Pore Diameters (14-23 nm). *J. Am. Chem. Soc.* **2010**, 132, 4438.
- (26) Ferber, J.; Luther, Computer Simulations of Light Scattering and Absorption in Dye-Sensitized Solar Cells. *J. Sol. Energy Mater. Sol. Cells* **1998**, 54, 265-275.